A MESH-FREE METHOD APPROCAH FOR THE COMPUTATIONAL MODELING OF HIGH RATE FRACTURE OF MATERIALS

Koffi Enakoutsa
UCLA, Department of Mathematics Los Angeles, CA 90095

ABSTRACT

A cutting-edge hybrid approach, integrating the Finite Element Method (FEM) and Mesh Reproducing Kernel Method (RKPM), has been meticulously developed to provide a robust and accurate simulation of dynamic structural responses under extreme loading conditions—specifically, scenarios involving high-speed impacts and penetration challenges. This innovation introduces a dynamic coupling mechanism between FEM and RKPM, offering the flexibility to employ either pure FEM or RKPM individually or in tandem for computations. The methodology is ingeniously designed to dynamically transition a Finite Element (FE) domain into a mesh-free domain based on triggering criteria derived from the material model, employing point-wise nodal coupling. This unique approach brings several advantages over existing methods, particularly those converting finite elements into Smooth Particle Hydrodynamics particles. Key merits include:

1. *Enhanced Accuracy in Crack Regions: The incorporation of RKPM in crack-prone areas significantly boosts accuracy compared to traditional methods.*
2. *Natural Evolution Triggers: Utilizing evolution triggers inherent to physics-based material models ensures a seamless integration that aligns with the underlying physical principles.*
3. *Computational Efficiency: By strategically leveraging finite elements in non-fracture regions, the methodology optimizes computational efficiency.*

This adaptive technique employs damage indicators from the material model to dynamically and automatically guide the conversion of elements from finite elements to RKPM. Notably, its versatility extends to any validated physics-based material model. A noteworthy example is the application of this methodology to a visco-plasticity/damage model, such as the BCJ model developed at Sandia National Laboratories. The BCJ model adeptly captures plastic deformation and failure in metallic materials subjected to high-rate events.

This work evaluates the predictive capabilities of the FEM/RKPM methodology, specifically in forecasting fracture occurrences in benchmark steel fracture scenarios utilizing the BCJ model. Furthermore, an assessment of the methodology's performance with a concrete model is thoughtfully presented, highlighting its broad applicability across diverse material representations.

INTRODUCTION

The KC-FEMFRE analysis code provides a coupled formulation of finite element (FE) and meshfree (MF) methods that is especially suited for analysis of transient dynamic responses of three-dimensional structures where extremes in response are anticipated. The intent in developing this code is to obtain a robust analysis method that can capture the sorts of extreme behaviors such as occur when a projectile penetrates concrete or rock.

From among the family of meshfree methods, the reproducing kernel particle method–(RKPM) was selected for the MF method to be employed in the KC-FEMFRE code. The RKPM formulation represents a relatively recent meshfree technology that has several key advantages in a coupled code environment, for instance the high degree of compatibility between RKPM and the FE method (FEM), particularly that they can employ the same material models. The coupling between FEM and RKPM is implemented in a controllable and evolutionary fashion (Wu, Magallanes, Choi, & Crawford, 2013) such that the code can perform pure FEM, pure RKPM or coupled FEM/RKPM calculations.

Generally when using the evolutionary coupling feature of KC-FEMFRE, at the outset the whole domain is discretized with an FEM approximation. If as the simulation proceeds, though, some portion of the FEM domain becomes severely distorted, it is converted into an MF approximation. This is done gradually based on using a limit or triggering criteria. Triggering criteria that have proved particularly effective are those generated from the state variables produced by material models—for example, the magnitude of damage exhibited by the K&C concrete (KCC) model (Crawford, Wu, Choi, Magallanes, & Lan, 2011) for a specific material point, which ranges from 0 to 2 as an analysis proceeds.

Finding an effective triggering criteria, one that triggers the evolution in a timely and efficient manner is important to developing a robust evolutionary formulation for predicting response to extreme events such as are represented by the penetration of solids by projectiles traveling at high velocities. Using triggering criteria, such as defined by one or combinations of the state variables provides a direct means to gauge the difficulty of the analysis at a particular material point. It also provides a detailed and localized look at the problem domain in terms of identifying the portions where the FEM formulation is likely to run into difficulty.

The efficacy of the FEM/RKPM methodology has been demonstrated for impact-type applications through comparison with experimental data, predominantly focused on concrete penetration, for which the K&C concrete model was utilized. The authors of this paper propose to broaden the validation methodology to encompass metallic materials, including Aluminum 6061-T6 and steel, for which a large database of mechanical data and constitutive material models already exist. To further advance the development of the meshfree code the authors implement a visco-plastic and damage internal state variable model. This model addresses void nucleation, growth, and coalescence, which when implemented within a meshfree code, presents significant benefits for problems associated with metal fracture and fragmentation, where extant material models and codes appears woefully inadequate. Also, advances in the development of the K&C concrete material model, including the ability to independently track tensile and compressive damage within

the meshfree computation will also be introduced, with comparison against extant concrete material models and test data provided. The paper is organized as follows.

- A review of the FEM/RKPM formulation and its numerical implementation are briefly described in Section 1.
- Section 2 presents the constitutive relations for both the steel and concrete material models.
- Finally, Section 3 the simulation of several benchmark problems to demonstrate the feasibility of the methodology.

FEM/RKPM FORMULATION AND NUMERICAL IMPLEMENTATION

FEM usually uses piece-wise linear shape functions, which produce a C^0 approximation. In contrast, RKPM uses first order complete basis for its shape function, which produces a C^1 approximation. Therefore, provided that the domain integration algorithms are exactly the same for the two methods, the FEM is more efficient but less accurate (because of the lower order shape functions), and the RKPM is more accurate but less efficient (due to its higher order approximation). Coupling of these two formulations could provide an approximation with both improved efficiency and accuracy.

An automatic, point-wise coupling scheme was implemented in the KC-FEMFRE code for coupling the FE and RKPM formulations. This scheme, a simple linearized combination of the two formulations was found, after several trial and error studies, to produce the best results in capturing the motions transmitted across the boundary between the two methods. This coupling process is described in Section 2.1. The RK and FE formulations employed are described in Sections 2.2 and 2.3.

Point-wise Coupling Scheme

Numerical approximation of an arbitrary function $f(\mathbf{x})$, denoted by $\hat{f}(\mathbf{x})$, can be written as:

$$\hat{f}(\mathbf{x}) = \sum_{I=1}^{NP} \Phi_I(\mathbf{x}) f_I$$

where $\Phi_I(\mathbf{x})$ is the shape function of node I evaluated at point $\mathbf{x}$, f_I is the coefficient of the approximation at node I, and NP is the number of nodes that are used in the discretization of the problem domain.

The approximation is the classical finite element approximation if $\Phi_I(\mathbf{x})$ is constructed based on elements connected by the NP nodes; on the other hand, the approximation is the reproducing kernel (RK) approximation if $\Phi_I(\mathbf{x})$ is constructed based on the NP discrete nodes with reproducing conditions enforced; and it would be a coupled approximation if $\Phi_I(\mathbf{x})$ is constructed by coupling the FE and RK shape functions.

The coupled shape function must satisfy partition of unity to ensure convergence and accuracy of the numerical approximation. Noticing that FE and RK shape functions satisfy partition of unity respectively, a simple combination of FE and RK shape functions can be taken as follows.

$$\Phi_I(\mathbf{x}) = (1-R)N_I(\mathbf{x}) + R\cdot\phi_I(\mathbf{x})$$

where $\Phi_I(\mathbf{x})$ is the coupled shape function of node I evaluated at point $\mathbf{x}$; $N_I(\mathbf{x})$ is the FE shape function; $\phi_I(\mathbf{x})$ is the RK shape function; and $R(0 \le R \le 1)$ is the coupling function. The coupled shape function $\Phi_I(\mathbf{x})$ satisfies partition of unity automatically.

The coupled simulation starts with FEM for the whole problem domain and then the FEM nodes are dynamically converted to RKPM nodes based on triggering criterion. As long as the same integration technique is applied for both FEM and RKPM domains, the FEM–RKPM conversion can be performed directly, i.e, using RK shape functions to replace FE shape functions directly when the conversion is carried out. To maintain the unique property of particle method so that debris generated from a fragmentation process can be tracked naturally, a nodal based unique domain integration technique is applied to integrate the weak form of the coupled approximation.

The coupling scheme is graphically illustrated in Figure **1**. The point-wise coupling indicates that each (integration) point defines a coupling zone. As shown in the figure, the coupling function R starts with zero for all nodes so that the whole domain is approximated by FE formulation. As the triggering criterion is satisfied, for example, at points $\mathbf{x}_I$, $\mathbf{x}_J$ and $\mathbf{x}_K$, R at these points are set to unity and three coupling zones are defined.

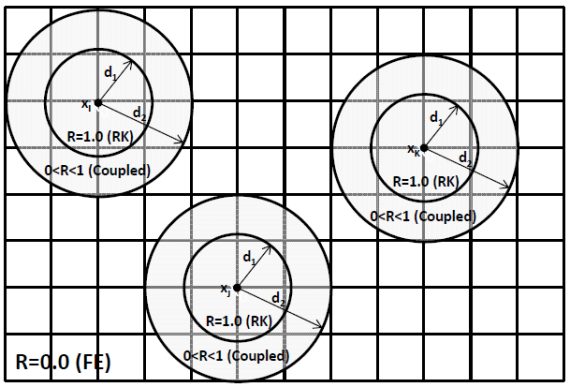

Figure 1: Various coupling domains defined by nodes I, J and K.

The coupling procedure is as follows: R at $\mathbf{x}_I$ is set to unity when the triggering criterion at node (integration point) $\mathbf{x}_I$ is satisfied, and subsequently, the nodes within the region covered by the sphere (circle in two-dimension) with radius of d_1 (no less than the support size of node $\mathbf{x}_I$) are converted to RKPM nodes; the nodes outside the region covered by the sphere with radius of d_2 (user adjustable, by default, $d_2 = 1.2d_1$) are maintained to be FEM nodes; the nodes between the two spheres are assigned as coupled FEM/RKPM nodes with the coupling parameter R being defined as:

$$R = \frac{d_2 - d}{d_2 - d_1}$$

where d is the distance between the nodes (in the coupling zone) and node $\mathbf{x}_I$ and coupled shape functions for these nodes are constructed. By defining the coupling function R in this manner, it varies linearly from FEM domain to RKPM domain, and this ensures the smooth transition between FE and RK approximations.

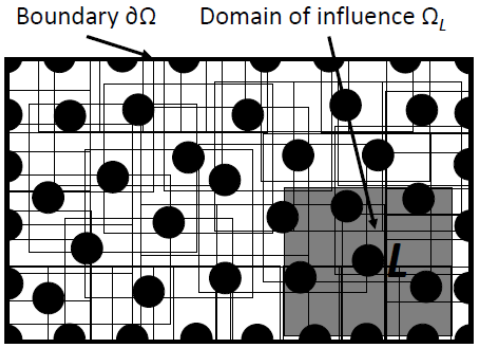

Figure 2: Meshfree domain discretization and domain of influence.

Lagrangian Reproducing Kernel Shape Function

The Lagrangian reproducing kernel (RK) approximation of an arbitrary function $u(\mathbf{x})$, denoted by $\tilde{u}(\mathbf{X})$, can be expressed as

$$\tilde{u}(\mathbf{X}) = \sum_{I=1}^{NP} \phi_I(\mathbf{X}) u_I$$

where NP is the number of particles used in the discretization, u_I is the coefficient of the approximation at node I, and $\phi_I(\mathbf{X})$ is the RK shape function evaluated at point $\mathbf{X}$. The RK shape function is constructed by a multiplication of enrichment function and kernel function as follows:

$$\phi_I(\mathbf{X}) = \Theta(\mathbf{X} - \mathbf{X}_I)\varphi_a(\mathbf{X} - \mathbf{X}_I)$$

The term $\Theta(\mathbf{X} - \mathbf{X}_I)$ is called the enrichment function and $\varphi_a(\mathbf{X} - \mathbf{X}_I)$ is the kernel function, which defines the smoothness and locality of the approximation, with a compact support Ω_I measured by a (which can be directionally different in multi-dimension problems). A commonly used kernel function is the cubic B-spline function, which gives C^2 continuity (smoothness).

$$\varphi_a(\mathbf{X} - \mathbf{X}_I) = \begin{cases} 2/3 - 4z^2 + 4z^3 & for \quad z \le 1/2 \\ 4/3 - 4z + 4z^2 - 4/3z^3 & for \quad 1/2 < z \le 1 \\ 0 & for \quad z > 1 \end{cases} \qquad z = |\mathbf{X} - \mathbf{X}_I| / a$$

The compact support a defines the unique small region for node L where its shape function is non-zero. The union of all the kernel supports should cover the entire problem domain. The black dots represent nodes, and the rectangle centered at the node stands for its support. The kernel support is truncated at the geometrical boundary of the problem domain. The support size a must be big enough so that the domain of influence overlaps each other and thus the moment matrix is constant.

KCC MATERIAL MODEL

Objective Stress Formulation

In the KCC model the evolution of the stress state follows an elastoplasticity law, where the elastic stage is assumed to be isotropic and in the plastic range the KCC model is adopted to describe the failure of the concrete. To accommodate the large deformation finite rotation effect, the Jaumann's objective rate $\boldsymbol{\sigma}^{\nabla}$ is employed:

$$\overset{\circ}{\boldsymbol{\sigma}} = \dot{\boldsymbol{\sigma}} - \boldsymbol{W}^{e}\boldsymbol{\sigma} + \boldsymbol{\sigma}\boldsymbol{W}^{e} = \boldsymbol{C}^{ep} : \dot{\boldsymbol{D}}$$

with

$$\dot{\boldsymbol{D}} = \frac{1}{2}\left(\boldsymbol{L} + \boldsymbol{L}^{T} \right)$$

$$\boldsymbol{W} = \frac{1}{2}(\boldsymbol{L} - \boldsymbol{L}^{T})$$

$$\boldsymbol{L} = \tilde{\mathrm{N}}_{x}\dot{\boldsymbol{u}}$$

where $\dot{\boldsymbol{D}}$ and $\boldsymbol{W}$ are the rate of deformation tenor and the spin tensor, respectively. $\boldsymbol{L}$ is the velocity gradient. $\boldsymbol{C}^{ep}$ is the elasto-plasticity tensor.

The rate of deformation tensor $\dot{\boldsymbol{\varepsilon}}$ can be decomposed into the elastic part $\dot{\boldsymbol{D}}^{e}$ and the plastic part $\dot{\boldsymbol{D}}^{p}$:

$$\dot{\boldsymbol{D}} = \dot{\boldsymbol{D}}^{e} + \dot{\boldsymbol{D}}^{p}$$

Failure Surface of the KCC Model

The concrete failure behavior is characterized by the pressure dependent yield surface defined as:

$$\mathrm{F}\ (p, \boldsymbol{\sigma}, \lambda) = \sqrt{3J_{2}} - \mathrm{R}\ \left(p, J_{3}, \lambda \right) \le 0$$

where p is the pressure (compression in positive) governed by equation of state, which represents volumetric responses. J_2 and J_3 are the second and third invariants of the deviatoric stress tensor, i.e., $J_2 = tr(\mathbf{s}:\mathbf{s})$, $J_3 = det(\mathbf{s})$. $\mathbf{s}$ is the deviatoric part of $\boldsymbol{\sigma}$, i.e., $\mathbf{s} = \boldsymbol{\sigma} + p\mathbf{I}/3$. They account for deviatoric responses. $\mathrm{R}\left(p, J_{3}, \lambda \right)$ is the failure surface given by:

$$\mathrm{R}\left(p, J_3, \lambda\right) = \begin{cases} r_f \cdot r\left(J_3\right) \cdot \left[\eta\left(\lambda\right) \cdot \left(\hat{\sigma}_m\left(p\right) - \hat{\sigma}_y\left(p\right)\right) + \hat{\sigma}_y\left(p\right)\right] & \lambda \le \lambda_m \\ r_f \cdot r\left(J_3\right) \cdot \left[\eta\left(\lambda\right) \cdot \left(\hat{\sigma}_m\left(p\right) - \hat{\sigma}_r\left(p\right)\right) + \hat{\sigma}_r\left(p\right)\right] & \lambda \ge \lambda_m \end{cases}$$

with

$$\hat{\sigma}_i\left(p\right) = a_{0i} + \frac{p}{a_{1i} + a_{2i} p} \qquad i = m, y, r$$

in which λ is the internal damage variable which is a function of effective plastic strain. r_f is the dynamic increasing factor (DIF) for strain rate enhancement, which is interpolated from the user input DIF curve. $\hat{\sigma}_m$, $\hat{\sigma}_y$ and $\hat{\sigma}_r$ are the three independent strength surfaces, namely, maximum strength surface, yield strength surface and residual strength surface, and the nine parameters (i.e., a_{0i}, a_{1i}, and a_{2i}) to define the three strength surfaces are calibrated from test data. Figure **3** shows the three independent strength surfaces for a generic concrete with unconfined compressive strength of 41.4 MPa.

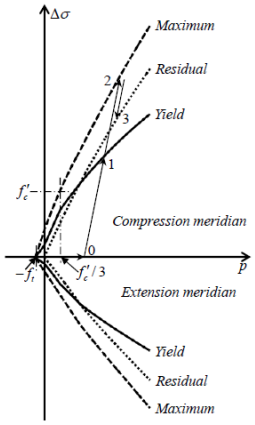

Figure 3: The independent strength surfaces for the KCC model.

$r\left(J_3\right)$ is the function proposed to effectively model the brittle-ductile transition of concrete under low to high confinements. $\eta(\lambda) \in [0,1]$ is an interpolation function that changes from zero to unity for $\lambda \le \lambda_m$ and from unity to zero when $\lambda \ge \lambda_m$ with $\eta(\lambda_m) = 1.0$. This procedure corresponds to the failure surface migrating from yield surface to maximum surface and then to residual surface, therefore, strain hardening and softening behaviors are efficiently modeled.

Damage Evolution in the KCC Model

The plastic flow is given by:

$$\dot{\boldsymbol{D}}^p = \dot{\mu} \frac{\partial \mathrm{G}(\boldsymbol{\sigma}, \lambda)}{\partial \boldsymbol{\sigma}}$$

with the plastic potential $G(\boldsymbol{\sigma})$:

$$G(\boldsymbol{\sigma},\lambda)=\sqrt{3J_2}-\theta R\left(p,J_3,\lambda\right)\le 0$$

in which $\dot{\mu}$ is the plasticity consistency parameter; θ is the associativity parameter while $\theta=1$ gives an associative plasticity and otherwise a partially associative formulation is invoked. For unconfined concrete, the default is $\theta=0.5$. The evolution of the internal damage variable I is defined as a function of the plastic rate of deformation tensor:

$$\dot{\lambda}=h(\boldsymbol{\sigma})\dot{\bar{D}}^p$$

with $\dot{\bar{D}}^p=\sqrt{\frac{2}{3}\dot{\boldsymbol{D}}^p:\dot{\boldsymbol{D}}^p}$. $h(\boldsymbol{\sigma})$ is the damage evolution factor:

$$h(\boldsymbol{\sigma})=\begin{cases}\dfrac{1}{r_f\left(1+p/r_f f_t\right)^{b_1}} & p\ge 0\\ \dfrac{1}{r_f\left(1+p/r_f f_t\right)^{b_2}} & p<0\end{cases}$$

with b_1 and b_2 being the material parameters calibrated from test data, and f_t is the tensile strength of the concrete.

BAMMAN-CHIESA-JOHNSON (BCJ) MODEL

Plasticity and Damage Modeling

The BCJ model is a physics-based plasticity, damage, and fracture material model rooted in J_2 deviatoric plasticity theory. The damage evolution is based on a void growth model, which is coupled to the plastic flow that provides for degradation of the elastic moduli. The BCJ model also incorporates path, strain rate, temperature and history effects through the use of internal state variables.

The formulations and expressions used to effectuate the BCJ model are described below.

- *Hypo-elasticity Law*

A hypo-elasticity law connecting the elastic strain rate to an objective time-derivative Cauchy-stress tensor given by:

$$\overset{\circ}{\boldsymbol{\sigma}}=\dot{\boldsymbol{\sigma}}-\boldsymbol{W}^e\boldsymbol{\sigma}+\boldsymbol{\sigma}\boldsymbol{W}^e=\left(1-\varphi\right)\left[\lambda tr\left(\boldsymbol{D}^e\right)\boldsymbol{I}+2\mu\boldsymbol{D}^e\right]-\left(\frac{\dot{\varphi}}{1-\varphi}\right)\boldsymbol{\sigma}$$

where λ represents the Lame constant, μ, the shear modulus, θ, the temperature, ϕ, the damage parameter, $\boldsymbol{W}^e$ the elastic spin. Note that the rigid body rotation is included in the elastic spin;

therefore, the constitutive model is expressed with respect to a set of directors whose directions are defined by the plastic deformation.

Also, the partition of the stress into its hydrostatic and deviatoric components leads to the governing equations for the pressure and the Jaumann rate of the deviatoric stress:

$$\begin{cases} \dot{p} = (1-\varphi)\kappa tr(\boldsymbol{D}^e) - \dfrac{\dot{\varphi}}{1-\varphi} p \\ \overset{\circ}{\boldsymbol{\sigma}}' = 2(1-\varphi)\mu \boldsymbol{d}^e - \dfrac{\dot{\varphi}}{1-\varphi}\boldsymbol{\sigma}' \end{cases}$$

where κ is the bulk modulus, and $\boldsymbol{D}^e$ is the elastic part of the deviatoric deformation defined by

$$\boldsymbol{d}^e = \boldsymbol{D} - \tfrac{1}{3} tr(\boldsymbol{D})$$

- *Flow Rule*

Next, the flow rule for $\boldsymbol{D}^p$ and $\boldsymbol{D}^d$, and the stretching rate due to the unconstrained thermal expansion $\boldsymbol{D}^{th}$, are introduced in addition to the equation for the plastic spin $\boldsymbol{W}^p$. From the kinematics, the dilatational plastic part $\boldsymbol{D}^d$ is given by

$$\boldsymbol{D}^d = \frac{\dot{\varphi}}{1-\varphi}\boldsymbol{I}$$

Assuming isotropic thermal expansion, the unconstrained thermal stretching rate $\boldsymbol{D}^{th}$ can be expressed as

$$\boldsymbol{D}^{th} = A\dot{\theta}\boldsymbol{I}$$

where A is a linearized expansion parameter.

For the plastic flow rule, a deviatoric flow rule is assumed and defined as

$$\begin{cases} \boldsymbol{D}^p = \sqrt{\tfrac{3}{2}} f(\theta) \sinh\left[\dfrac{\|\boldsymbol{\xi}\| - (1-\varphi)\left[\kappa + Y(\theta)\right]}{(1-\varphi)V(\theta)}\right]\dfrac{\boldsymbol{\xi}}{\|\boldsymbol{\xi}\|} \\ \boldsymbol{\xi} = \boldsymbol{\sigma}' - \tfrac{2}{3}\boldsymbol{\alpha} \end{cases}$$

where θ represents here also the temperature, κ the scalar hardening variable, $\boldsymbol{\sigma}'$ is the deviatoric Cauchy stress, and $\|\boldsymbol{X}\|$, the magnitude of any arbitrary second order tensor $\boldsymbol{X}$. There are several

choices for the form of the plastic spin $\boldsymbol{W}^p$. The assumption that $\boldsymbol{W}^p$=0 allows recovering the Jaumann stress rate.

- *Hardening Evolution Law*

The evolution equations for the isotropic and kinematic hardening internal state variables are given in a hardening minus recovery format:

$$\begin{cases} \overset{o}{\boldsymbol{\alpha}} = \dot{\boldsymbol{\alpha}} - \boldsymbol{W}^e\boldsymbol{\alpha} + \boldsymbol{\alpha}\boldsymbol{W}^e = h(\theta)\,\boldsymbol{D}^p - \left[\sqrt{\frac{2}{3}} r_d(\theta)\left\|\boldsymbol{D}^p\right\| + r_s(\theta)\right]\|\boldsymbol{\alpha}\|\boldsymbol{\alpha} \\ \dot{\kappa} = H(\theta)\left\|\boldsymbol{D}^p\right\| - \left[\sqrt{\frac{2}{3}} R_d(\theta)\left\|\boldsymbol{D}^p\right\| + R_s(\theta)\right]\kappa^2 \end{cases}$$

where h and H are the hardening moduli, r_s and R_s are scalar functions of θ describing the diffusion-controlled "static" or "thermal" recovery, r_d and R_d are the functions of θ describing dynamics recovery.

- *Damage Evolution Law*

The evolution equation for the damage is given by

$$\dot{\varphi} = \left[\frac{1}{(1-\varphi)^m} - (1-\varphi)\right]\sinh\left[\frac{(1-m)}{(1+m)}\frac{p}{\bar{\sigma}}\right]\left\|\boldsymbol{D}^p\right\|$$

where p and $\bar{\sigma}$ denote the pressure and the effective stress, respectively. Note that the evolution equation the damage displays a "*sinh*" dependence upon the triaxiality factor $\frac{p}{\bar{\sigma}}$, as well as an additional parameter "m" along with the initial value of the damage φ_0 required to calculate the damage growth. This reflects an implicit assumption of the model that damage must be preexisting to a small extent in order to evolve. Furthermore, it is assumed that only tensile state contribute to the damage growth. That is $\dot{\varphi}$=0 for compressive states of hydrostatic stress. To ensure this result, the pressure p in the evolution equation of the damage is limited to value greater than zero. As damage accumulated towards maximum value of 0.99 the deviatoric elastic and plastic strength degrade to trivial values. Thus, once the material has completely failed, it is no longer supporting any directional stress and effectively become fluid-like in its behavior.

- *Temperature Change*

The last equation to complete the description of the model is the one that computes the temperature change during high strain rate deformations, such as those encountered in high rate impact loadings. For these problems, a non-conducting (adiabatic) temperature change, following the assumption

that 90% of the plastic work is dissipated as heat, is assumed. The rate of the change of the temperature is assumed to follow

$$\dot{\theta} = \frac{0.9}{\rho C_v} \boldsymbol{\sigma} : \boldsymbol{D}^p$$

where ρ and C_v represent the material density and a specific heat coefficient, respectively.

NUMERICAL EXAMPLES

The capability of the KC-FEMFRE code is demonstrated based on two high rate deformation problem including the failure of a W14x132 4340 steel column subjected to a blast load. The dimensions of the specimen as well as its mesh discretization are presented below.

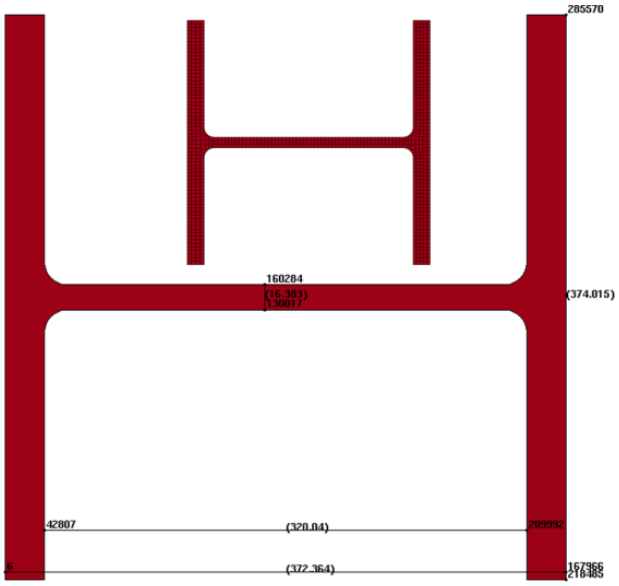

Figure 4: Dimensions of the W14x132 column specimen and its LS-DYNA mesh discretization.

The mechanical behavior of the W14x132 4340 steel under blast load is described using the BCJ model, as described above. Both the failure and plastic parameters of the BCJ model for the 4340 steel were calibrated based on temperature and strain rate dependence data found in the literature for this steel. This fitting procedure of the BCJ parameters is not discussed in this work. The pressure load was applied on both the web and the flange of the specimen. Elements were allowed to erode once the plastic strain reaches a critical value.

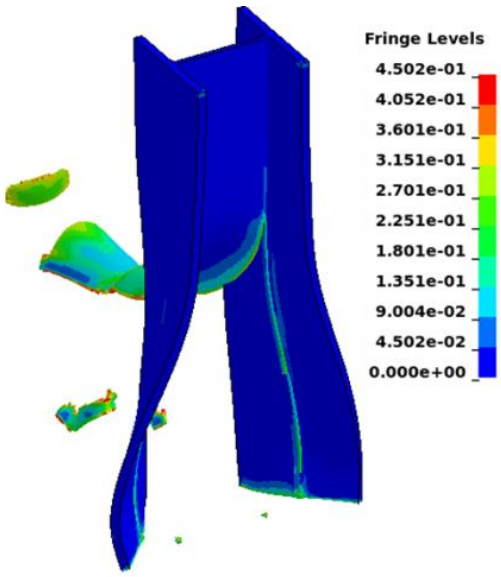

Figure 5: Distribution of the plastic strain in the deformed specimen using KC-FEMFREE code.

Figure **5** illustrates the fracture of the specimen predicted by the KC-FEMFREE code. The simulation shows several pieces of metal fragments that are detached from the column.

The second application of the KC-FEMFRE code (not necessary related to fracture) is the problem of the uniaxial compression of a concrete cylinder. As shown in Figure **6**, a diameter of 152.4 mm, height of 304.8 mm plain concrete cylinder is used in the unconfined compression test. The unconfined compressive strength of the concrete is 45.4 MPa. The bottom is completely fixed. The top is fixed laterally and pushed downward at a velocity of 25.4 mm/sec. Default KCC model except a constant b_1=0.62 for all the discretizations is used for the simulations.

Figure **7** shows the engineering stress – strain responses for the uniaxial compression test. From Figure **7**a, it is seen that with the adjusted b_1, the numerical results match test data quite well. If, on the other hand, a unique b_1 is used for all the discretizations, for example, b_1=0.62, mesh dependence is observed. However, this mesh dependence diminishes as confinement presents. Nevertheless, this observation suggests a thorough investigation of the regularization schemes for the KCC model in the meshfree nodal integration framework.

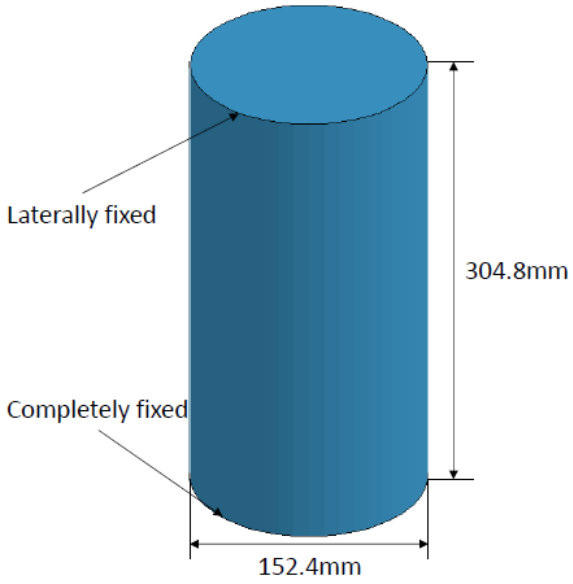

Figure 6: Specimen for cylinder uniaxial compression test.

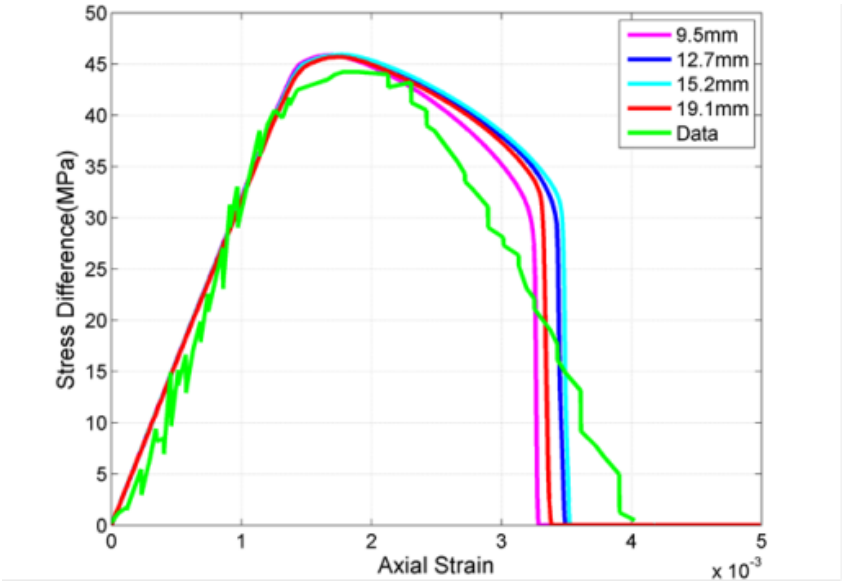

(a) b_1=0.40, 0.62, 0.72 and 0.85 respectively.

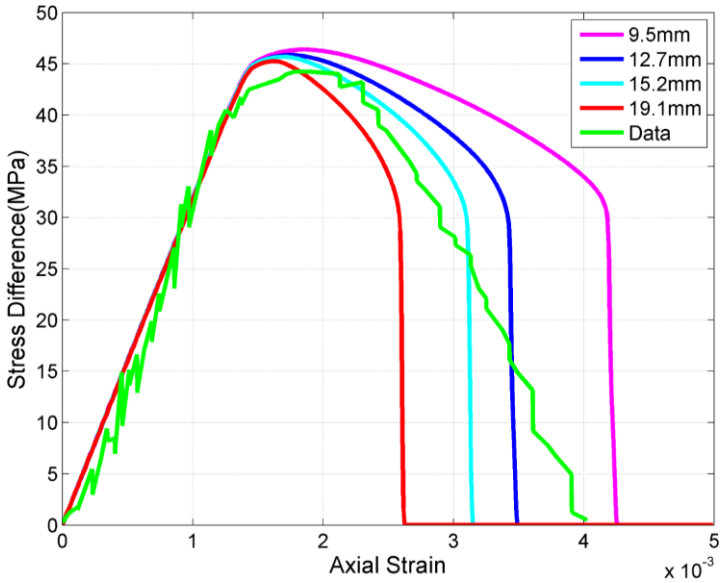

(b) b_1=0.62 for all discretizations.

Figure 7: Engineering stress-strain responses for cylinder compression test.

In this study the capability of the KC-FEMFRE code is demonstrated on metallic material under high rate deformation modelled by the BCJ model. A review of this assessment for concrete material is also provided.

REFERENCES

Crawford, J., Wu, Y., Choi, H., Magallanes, J., & Lan, S. (2011). *Use and Validation of the Release III K&C Concrete Material Model in LS-DYNA.* TR-11-36.6, Burbank.

Wu, Y., Magallanes, J., Choi, H., & Crawford, J. (2013). An Evolutionarily Coupled Finite Element - Meshfree Formulation for Modeling Concrete Behaviors under Blast and Impact Loadings. *ASCE Journal of Engineering Mechanics, 139*(4), p525-536.